Chapter 4 Determination of dye diffusion coefficient

4.1 Introduction

As addressed in Sub-Section 1.4, *stratum corneum* represents the main barrier to substance penetration or permeation to skin. In order to characterise the skin permeability, diffusion coefficient, *D* offers convenient means for its quantification. Diffusion coefficient provides useful information on material diffusion in highly heterogeneous skin, and factors influencing this diffusion. In particular, sampling *D* locally results in acquisition of a *D* - spatial map that is helpful for investigation of the major biological pathways in skin. Therefore, determination of the diffusion coefficient in skin locally, non-invasively, in real time, and, preferably, *in vivo*, will greatly assist the understanding of pharmacodynamic properties of skin, its resistivity to environmental toxins, and transdermal drug delivery vehicles.

In this Chapter, this important research topic will be addressed by demonstrating a method of determination of *D* in skin at a locality in the skin sample by using a fluorescent model of low-molecular-weight drugs. Demonstration of application of the fluorescence recovery after photo-bleaching (FRAP) technique to determination of *D* in skin will be reported.

FRAP technique basics and objectives

In FRAP, fluorescence recovery time-evolution is recorded and analysed at a sample locality, where the fluorescence was photobleached. The FRAP time-evolution curve is fitted with exponentials, whereby the exponential time constants provide parameters from which the local (i.e. in the photobleached area) *D* is determined. Since skin is a complex, highly heterogeneous structure, it is necessary, first, to establish the FRAP method using a simplified homogeneous fluorescence model. A plain glycerol mixture with organic fluorescent dye, Rhodamine B (Rh:B) was chosen as this homogeneous fluorescence model. This fluorescent medium possesses high viscosity comparable to that of the skin. This model was also preferred, as it has been described in the literature (Braga, 2004), where, in particular, Rh:B molecular size was measured by using TEM, which represented a critical parameter for calculation of *D*. The fitting accuracy represents a challenge of this method, and it depends critically on the shape and size of the photobleached volume (PBV). Photobleached depth (PBD, the vertical length of PBV) is an important parameter which can be experimentally determined by measuring the axial point spread function (axial PSF) of FMM. In FMM, it relates to excitation volume. Generally, elliptical shape of the bleached volume calls for a mathematical model that accounts for the ellipticity. This model is developed in the course of this project largely by efforts by Dr Anissimov, Griffith University.

In this Chapter, the development of the glycerol-Rh:B model, refinement of the method using the adapted mathematical model will be reported, and, for the first time to the best of the knowledge, its demonstration to measurement of the local diffusion coefficient in skin, and specifically, in *stratum corneum*.

In the study, FMM as an imaging modality was preferred to FCSM that was widely used in the FRAP prior-art. In the implementation of FMM, more power was afforded from the high-power femtosecond laser sources, which allowed rapid bleaching of the focal volume at a reduced off-focus photobleaching. All the FRAP results were obtained using the FMM system (Zeiss510, AIBN, University of Queensland) with a 63×, NA1.0, water-immersion objective lens. A suitable fitting model of the FMM FRAP data will be introduced, and its experimental demonstration will be reported.

4.2 Methods

4.2.1 Rh:B molecular radius

The radius of Rh:B can be calculated by the following formula:

$$R = \frac{1cm}{\sqrt[3]{\frac{s}{mw} NA}} \qquad 4)$$

where s is the density of Rh:B, mw is the molecular weight of Rh:B, measured in Da, and NA is the Avogadro's constant ($s = 0.79 g \cdot cm^{-3}$, $mw = 479.02 g \cdot mol^{-1}$, $NA = 6.023 \times 10^{23}$). Molecular radius of Rh:B is calculated to be ≈1 nm. Since TEM has an adequate resolution at the sub-nanometre scale, this instrument is resorted to of the Rh:B size.

TEM sample preparation

A small amount of Rh:B-powder (479.02 Da, density 0.79 g/cm^3, Sigma) was put into a high-purity grade ethanol. Rh:B/ethanol solution was centrifuged for best solubilisation. The use of ordinary grade ethanol was avoided, as it could introduce uncontrollable artefacts. 10-μL Rh:B ethanol solution was pipetted out and applied on the carbon coated grid with the stain (Uranyl Acetate, negative stain). Immediately after this, the grid was put on a filter paper for absorbing solution residue from the sample. Then, the grid was air-dried for several minutes. Finally, the sample on the grid was imaged using a TEM system (JEM-1010A, JEOL).

Since the molecular radius of Rh:B is on the nanometre scale of, high magnification was used for its determination: 600,000 and 500,000 times at a magnification 100 kV acceleration voltage.

4.2.2 Axial point-spread function

As mentioned in Introduction, axial point spread function (axial PSF) of the FMM system determines PBD. By definition, axial PSF is an optical system image of a point-like source, including a fluorescent source in context of this chapter. A light wave, which is a point source, will acquire wave front distortions when passing the optical system, so that when converging, it will form an extended spot. This spot can be of shape, as shown in Fig 60(a). There are two main reasons. Firstly, aberrations in the optical system will spread the image over a finite area. Secondly, diffraction effects will also spread the image, even in a system that has no aberrations.

It can be determined by using several methods. In this case, a 20-μm-thick sample of Rh:B solution was prepared that was sandwiched between microscope slide and glass cover slip plates. This sample was imaged at several depth intervals using FMM. The multiphoton fluorescence (MPF) signal intensity was plotted versus the depth (z-axis), as shown in Fig 59. It is straightforward to figure out that the axial PSF can be found by taking a derivative of this function with respect to the z-variable using Matlab-based program (see Fig 60 b)). Appendix II contains all of the program details. Full width at half maximum (FWHM) function of the curve in Fig 60 b) yielded the axial PSF of the optical imaging system. In case of the data presented in Fig 59, the axial PSF was determined to be 3 μm. Axial PSF is dependent mainly on the microscope setting: objective lens.

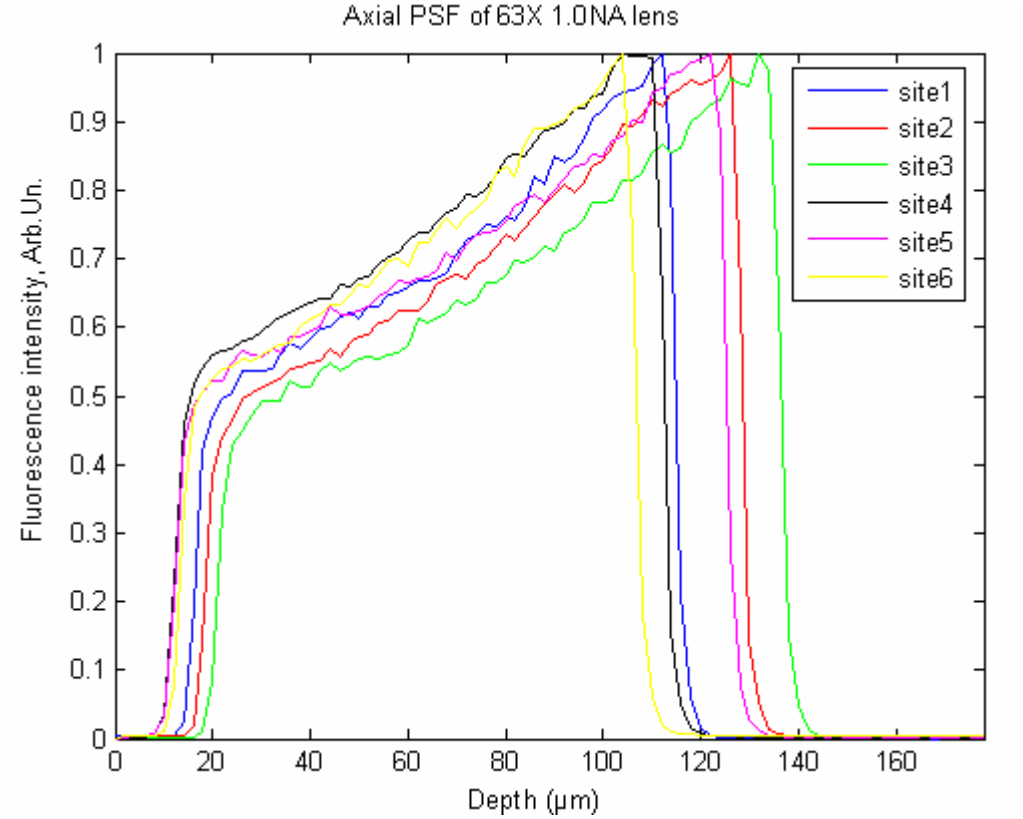

Fig 59. MPF signal intensity versus the depth (z-axis). x-axis (μm); y-axis: normalized Intensity

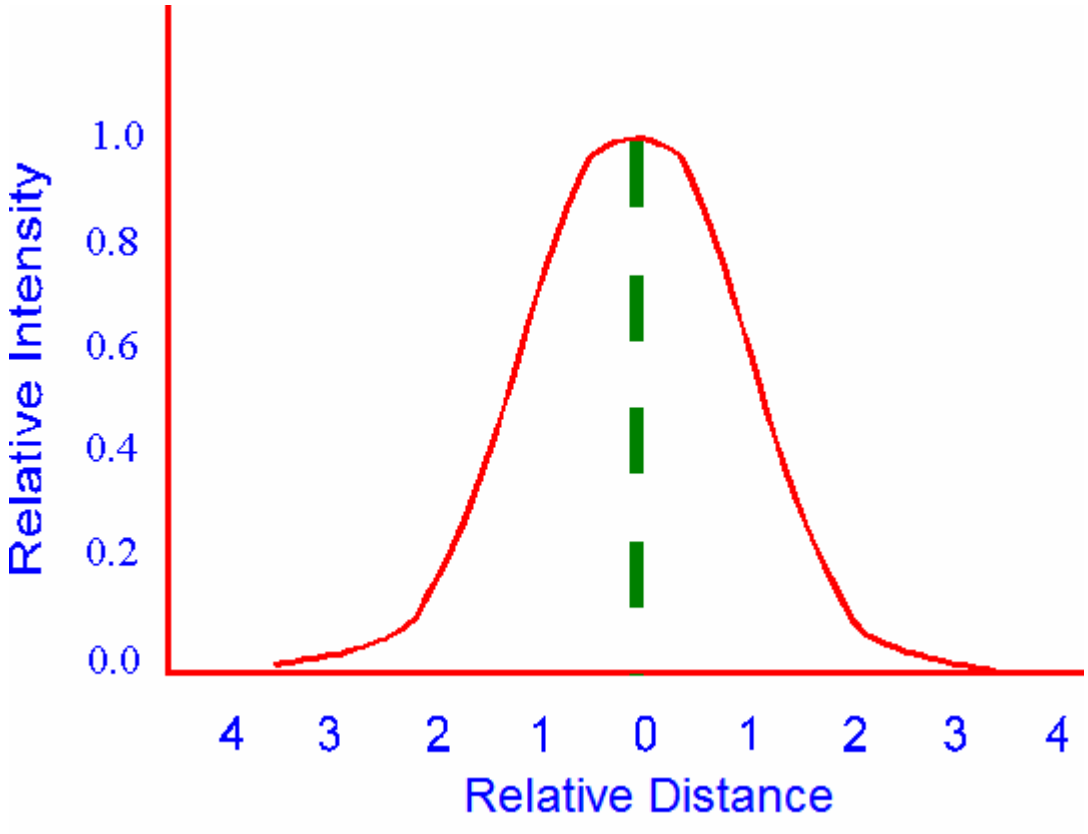

a)

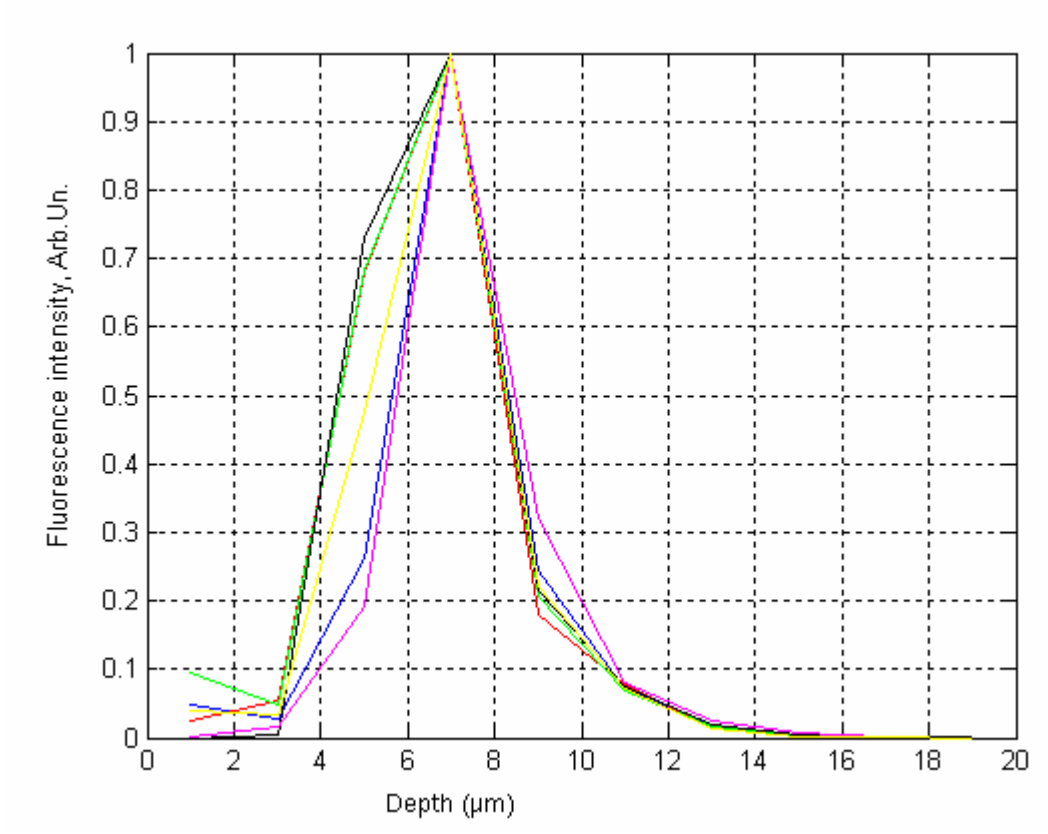

b)

Fig 60. a) Consider a very small point of light. If the visual system had perfect optics the image of this point would be identical to the original point of light. So if the relative intensity of this point of light were plotted as a function of distance, such a plot would look like the dashed, vertical line. However, the optical system is not perfect so the relative intensity of the point of light is distributed across image plane as shown by the curve. This curve is called the "point spread function" (PSF) b) A family of axial PSFs of the FMM imaging system featuring an 63×, NA1.0, water-immersion objective lens sampled at six different sites. x-axis (μm); y-axis, normalized Intensity. FWHW was measured to be 2.7±0.3 μm. It was primarily determined by the objective lens. In the context of the FRAP measurement the axial SPF is referred to as a PBD

Sample preparation

Firstly, 20 μL of 20 mM Rh:B solution was placed in 4-mL glycerol and mixed evenly to obtain 10 μM Rh:B solution in glycerol. 10 μL of this solution was applied on a microscope glass slide and sealed with a cover slip, followed by imaging using the FMM system.

FMM settings

A femtosecond laser operated at a mean wavelength of λ_{ex} = 810 nm (scanning power P_{sc}, around 33 mW,1% of the total laser out-put energy which was 3310mW) was employed as the excitation source. A bandpass filter centred at a wavelength of 560 nm (bandwidth, 60 nm) was used to transmit the Rh:B fluorescence to a detector. In order to induce photobleaching in

the sample, the laser pulse power used for photobleaching (P_{pb}) was raised to a value of about 165, 331, and 496 mW (5%, 10% and 15% of the total laser out-put energy which was 3310mW). The values of the laser power were set by the imaging software. The FMM imaging and photobleaching parameters were essentially the same for both glycerol/Rh:B model and skin FRAP experiments (see Fig 61).

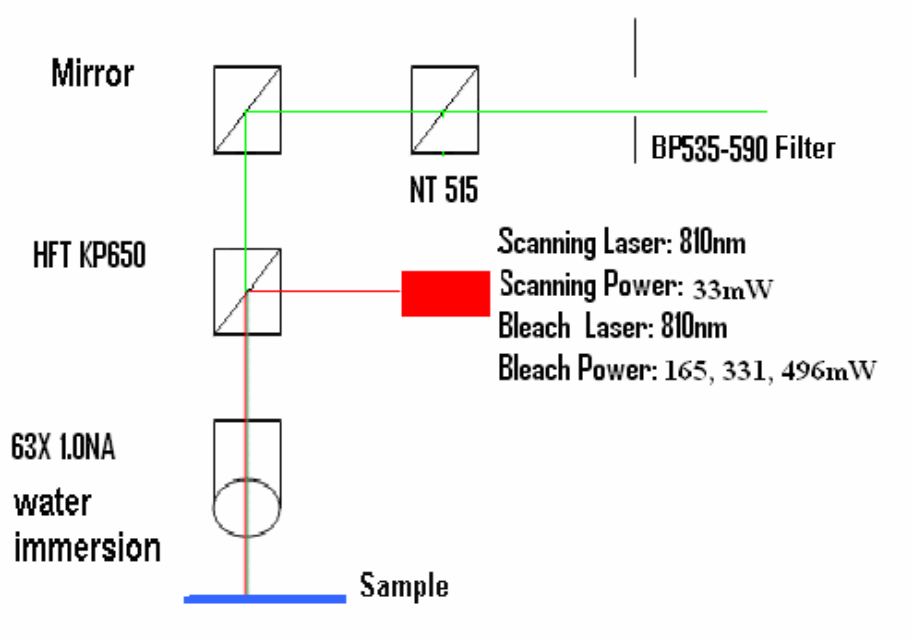

Fig 61. Schematic diagram of the FMM imaging system employed for the FRAP experiments: scanning laser power, P_{sc} = 33 mW; photo bleaching incremental laser power values were P_{pb} = 165, 331, 496 mW; HFT KP650, a dichroic mirror shortpass, with a wavelength cutoff λ_{cutoff} = 650 nm; NT515, an additional dichroic mirror shortpass λ_{cutoff} = 515 nm; BP535-590, bandpass filter, with the wavelength transmission band of 535 to 590 nm

4.2.3 Averaging method

As detailed in Chapter 1, Sub-Section 1.6.3, the FRAP method relies on probing a fluorescence signal within the PBV. As a result, recording and analysis of the fluorescence signal time-evolution provides means of determining the photobleaching recovery rate at PBV in the sample. A typical FRAP signal is presented in Fig 62, 'FRAP curve single run'. As one can see, this signal is noisy. In order to improve SNR, the FRAP signal was averaged over several runs. The averaging is especially important in case of a small photobleached area (PBA), e.g. 1×1 μm^2. In the experiments, 10 runs were typically required to attain a reasonable SNR.

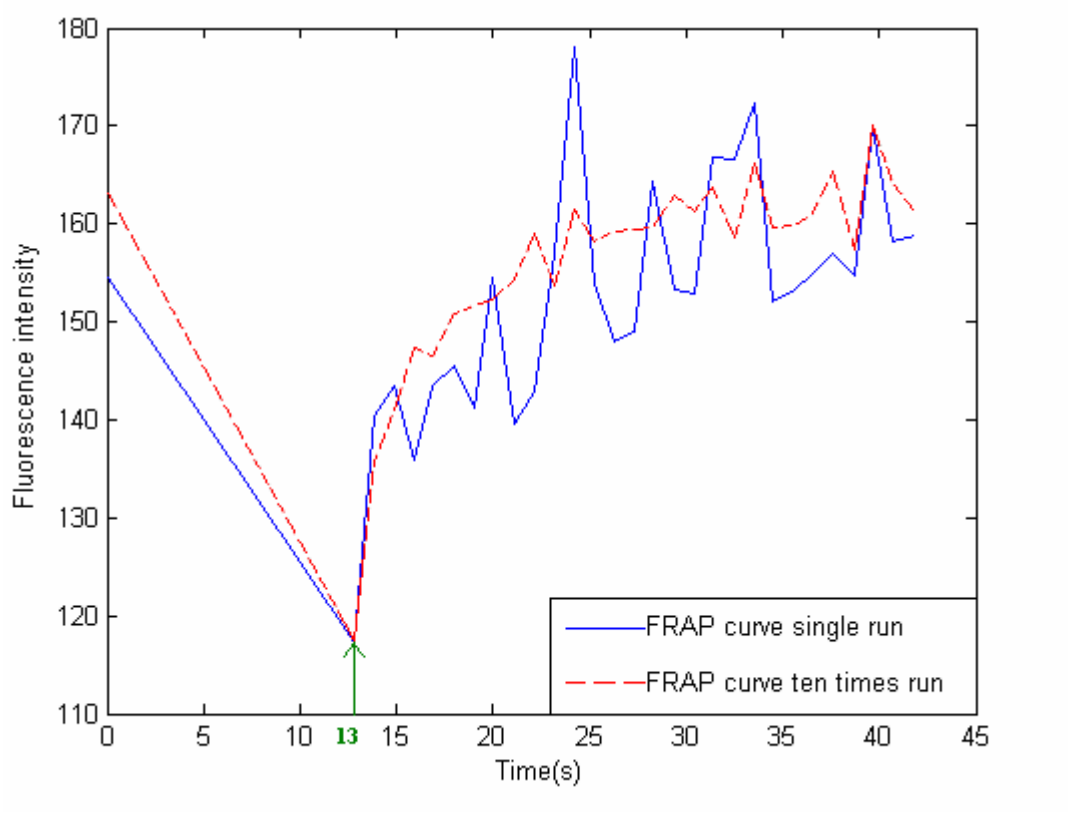

Fig 62. A typical experimental plot of the FRAP fluorescence data: fluorescence intensity versus time. High-power laser radiation was applied for the initial time interval of 13 s, manifested by the fluorescence intensity drop to the minimum level. The fluorescence recovery then commenced photobleaching at a time mark of 13 seconds. Blue (solid), red (dashed) curves represent single-run, 10-time average FRAP signals, respectively. The photobleached area diameter, d_{PBA} = 2 µm

4.2.4 FRAP in homogeneous medium

Sample preparation

10 µM glycerol/Rh:B solution was sandwiched and sealed between a microscope glass and cover slip that were separated by two spacers made of glass cover slips. As a result, a 170 µm thickness solution was prepared as a fluorescent homogeneous medium model for FRAP characterisation and refinement.

FMM settings

The equipment settings were as described in Sub-Section 4.2.2 "FMM settings". The excitation wavelength was chosen 810 nm (P_{sc} = 33 mW, P_{pb} = 165, 331, 496 mW). Image size was 27×3 µm^2. Time interval between two FRAP recordings was 30 ms. The photobleaching pulse duration was τ_{PB} = 282 ms. All the experiments were done at room temperature of 25 ^{0}C.

4.2.5 FRAP in *stratum corneum*

Sample preparation

The excised skin, *stratum corneum* only (female, aged 33, abdomen) was immersed in 10-μM Rh:B solution for 2 days to allow the dye spread evenly throughout the sample, followed by the skin placement on a slide and covered with a cover slip and sealing by nail polish.

FMM settings

The equipment settings were as described in Sub-Section 4.2.2 "FMM settings". The ultrashort pulse laser operated at λ_{ex} = 810 nm (P_{sc} = 16.5 mW, P_{pb} = 165 mW). Image size was 256×30 square pixels, with pixel size of 100×100 nm^2. The fluorescence imaging after photobleaching time interval was 30 ms. τ_{PB}= 282 ms. Experiments were carried out at room temperature of 25 ^{0}C.

4.3 Results

4.3.1 Rh:B molecular radius

The results of high-resolution TEM-imaging are presented in Fig 63.

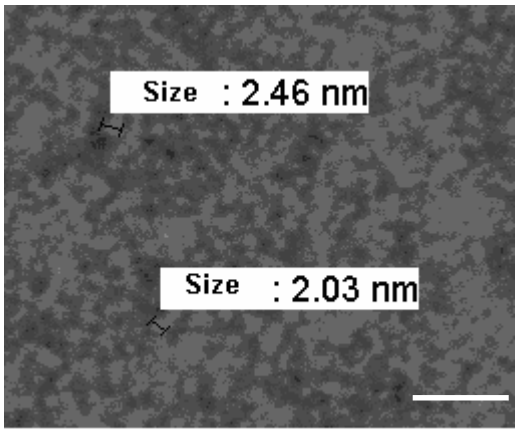

Fig 63. TEM image of Rh:B. The bright spots are Rh:B particles on a dark background due to the negative stain. An individual Rh:B molecule size is shown with a ranger (black cut). Scale bar 10 nm

It can be clearly seen that the Rh:B diameter ranges from 2 to 2.5 nm, which is at the TEM resolution limit of 2 nm. The averaged diameter is evaluated as 2.2 nm, which was in the excellent agreement with the calculated Rh:B radius of 1 nm.

4.3.2 Photobleached volume (PBV)

In order to apply the fitting parameters to the theoretical FRAP model, it was needed to know not both PBD and PBA but also the shape of PBV. An experimental method was devised to determine PBV. A micrometre-sized area in the skin sample was photobleached by its

exposure to 300 mW femtosecond laser radiation. A z-stack image set containing PBV was acquired at an interval of 1 μm (see Fig 64). The image processing and analysis yielded the PBV shape.

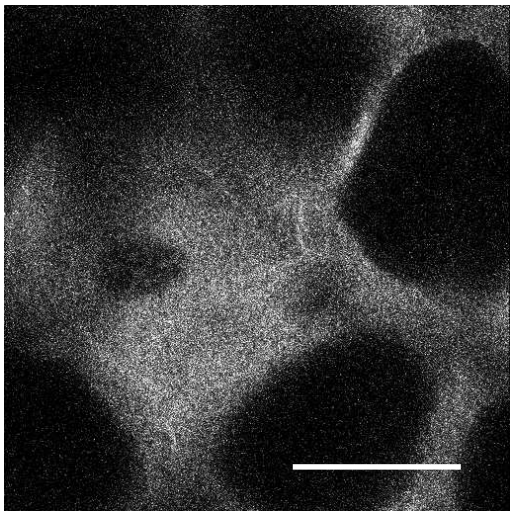

a)

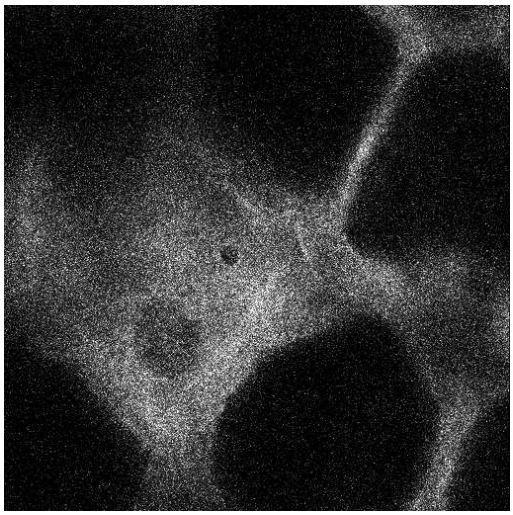

b)

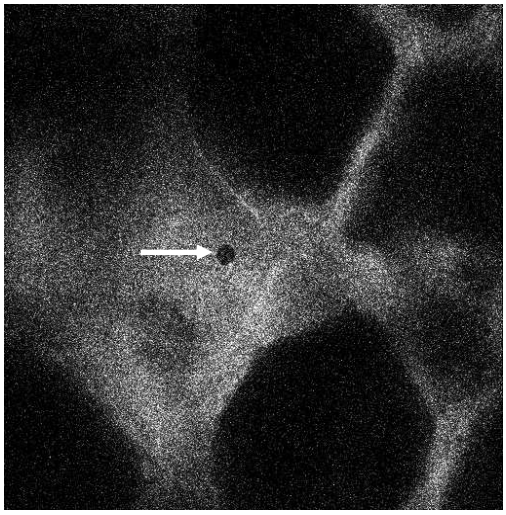

c)

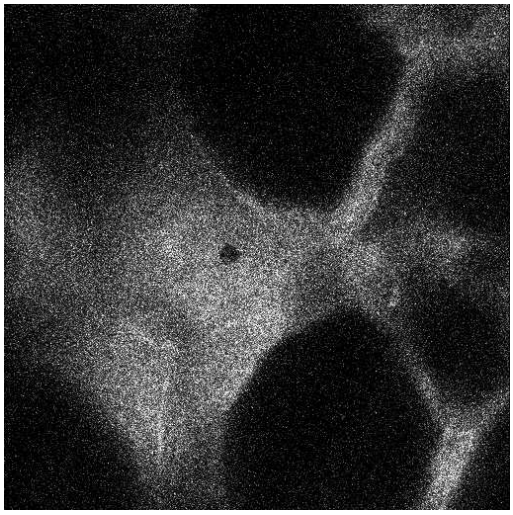

d)

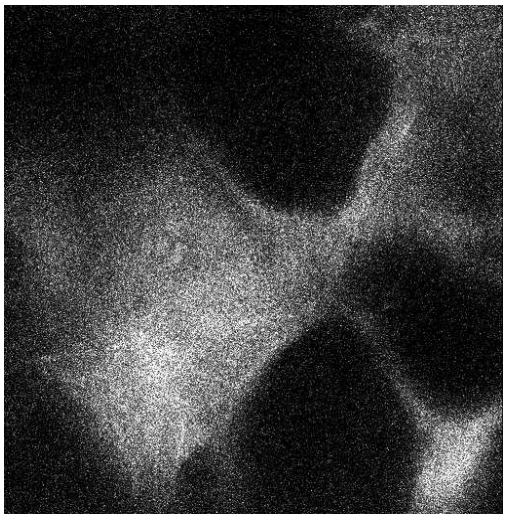

e)

Fig 64. Z-stack FMM image set of the skin sample with a PBV observable as a dark circle (pointed by a white arrow in image c). Images (a) to (e): an image set acquired from the skin top surface to the in-depth layer at an interval of 1 μm. Scale bar 30 μm

From these images, it can be seen that PBA was observed as a dark circle in the morphology layout image of skin and perpetuated throughout the images from (b) to (d), which amounted to 3 μm of the axial translation. This confirmed PBD = 3 μm. Also, by reconstruction of the 3D z-stack, the shape of PBV was determined as a prolate spheroid with a circular cross-section.

Fitting model

A fitting model based on the simplified assumption of the bleached volume parallelepiped-shaped was developed by Dr Anissimov using the Green's function approach. This model was initially used in fitting FRAP data of the glycerol/Rh:B, and proved to be most accurate among the other spheroid and ellipsoid models. After the experimental validation of this model, it was applied to the FRAP data on skin.

4.3.3 FRAP in homogeneous medium: glycerol

There are three factors that can vary in the FRAP experiments: photobleaching position in the sample, PBA, and P_{pb}. In the following part of this paragraph, results of testing of the FRAP method susceptibility to the incomplete photobleaching that might influenced by these three factors are presented. Incomplete photobleaching is referred to as a photobleaching process whereby a residual fluorescence signal remains at the completion of the photobleaching. FRAP signals at three axial positions in a Rh:B-glycerol sample of 170-μm thickness were recorded. The PBVs were located at the front surface, 1 - 2 μm from the top (near to the front interface of the sample), in the middle, 60 μm from the top, and at the bottom surface, 120 μm from the top (i.e. near to the bottom interface of the sample). Three different sizes of the circular bleached area were examined of radius 1μm (1 in table 6 and 7), 1.1μm (2 in table 6 and 7), and 1.25μm (3 in table 6 and 7). Three P_{pb} were applied: 165, 331 and 496 mW. The results of these FRAP image acquisition are presented in Fig 65.

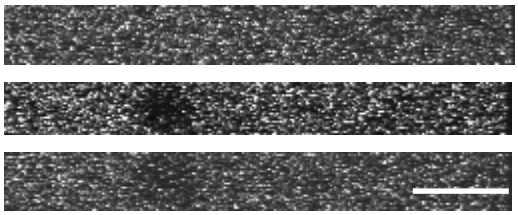

Fig 65. FRAP images from top to bottom: before photobleaching; 30 ms after photobleaching; 150 ms after photobleaching. The PBA is visible as a dark area of the circular shape (middle image). Scale bar 5 μm

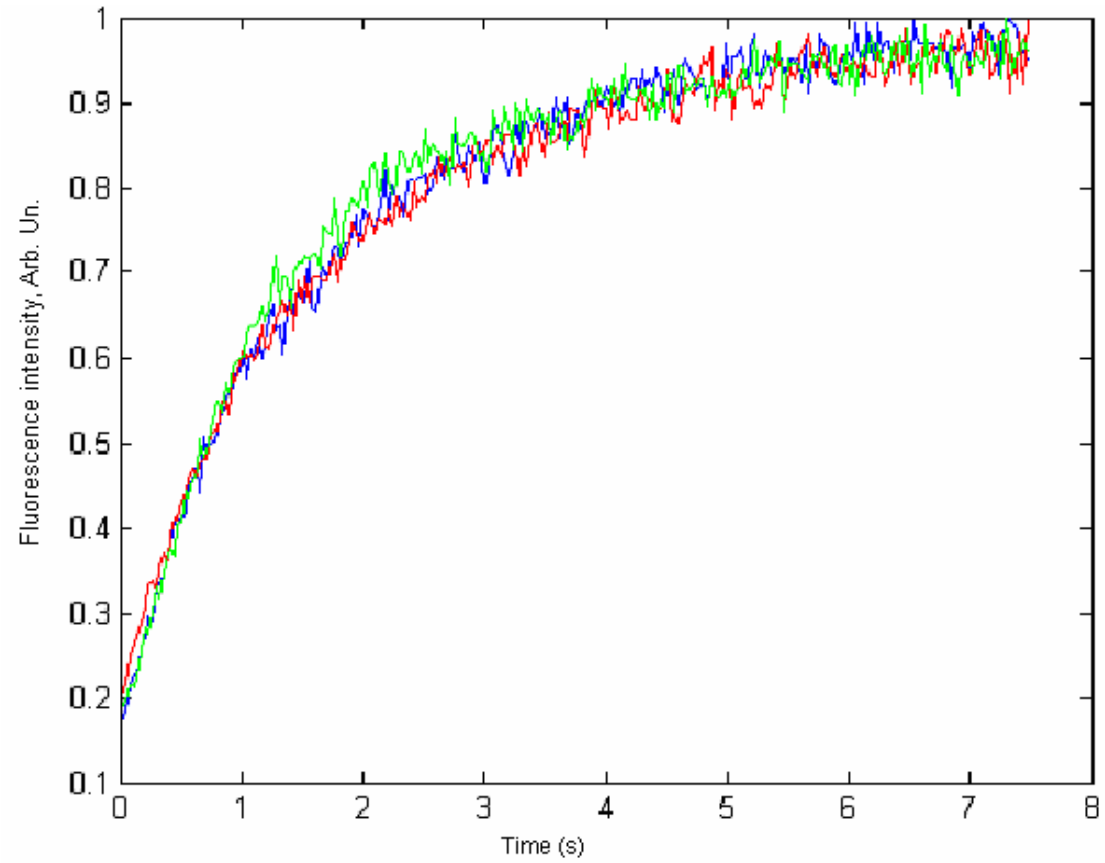

(a)

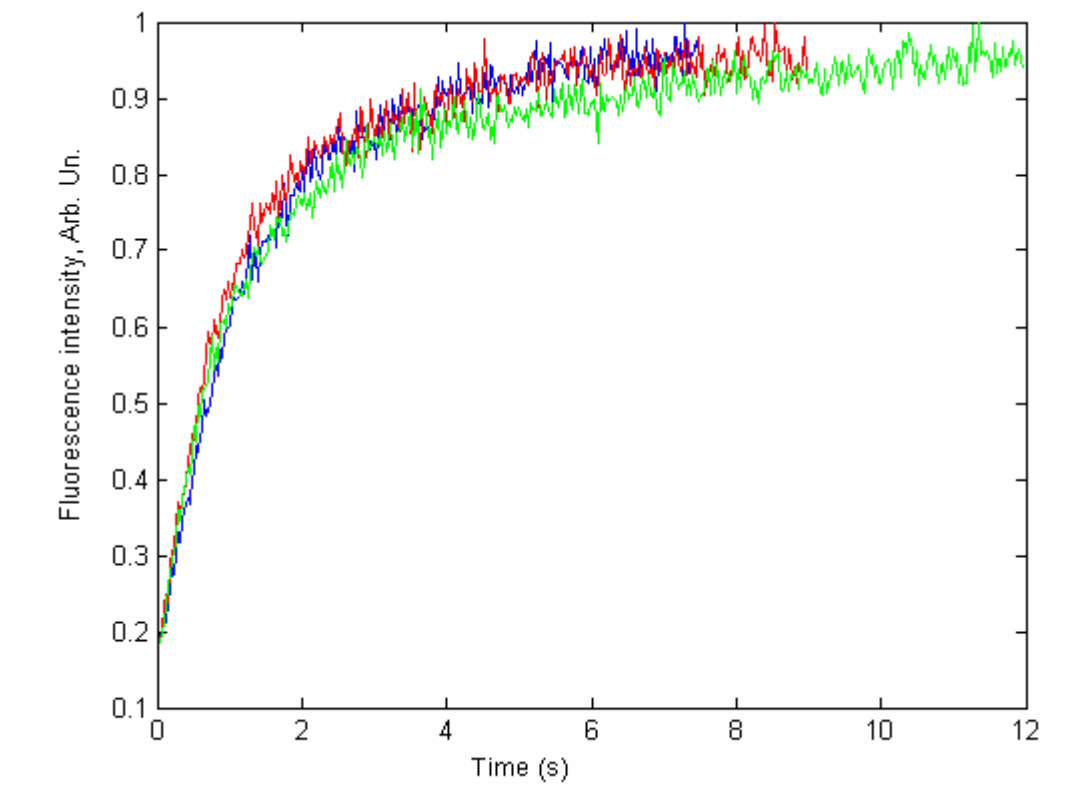

(b)

Fig 66. FRAP recordings versus time tested against the following parameters at P_{pb} = 496 mW: (a) PBA 1×1 μm^2 at depths in the sample: front surface, middle, and bottom surface, colour-coded green, red, and blue, respectively; (b) FRAP curves at the sample front surface for different PBAs of 1×1 μm^2,; 1.1×1.1 μm^2, and 1.26×1.26 μm^2, colour-coded blue, red, and green, respectively

Comparison of the normalised FRAP curves (see Fig 66) acquired at the varied parameters of PBAs and PBV locations showed the conclusion that FRAP signal was immune to PBA and PBV location in a sample. Also, the test of incomplete photobleaching of the sampling volume yielded essentially the same results for *D*. Photobleaching at P_{pb} = 165 mW and 331 mW yielded similar results as at 496 mW. That meant the incomplete photobleaching had little effect on the FRAP performance.

Data fitting results

In order to determine the diffusion coefficient, *D*, the following formula was employed:

$$D = \frac{k_B T}{6\pi\eta R} \quad \text{(Braga, Desterro } et\ al\text{. 2004)} \qquad 5)$$

Where k_B =1.38066 *10^{-23} J/K is the Boltzmann's constant

η =934*10^{-3} Pa·s (Glycerol) at 25^{0}C (Lide 1992-1993)

R=1 nm (Rh:B radius)

D, diffusion coefficient, measured in cm^2/s

The calculation yields = 2.4×10^{-9} cm^2/s.

Several PBV shapes were tried to achieve the best fitting results: sphere, prolate/oblate spheroids and cube. The FRAP fitting formula for a prolate spheroid model is characterized by two parameters: $a = h/2$ (Equation 1, Appendix III), and $a \neq h/2$ (Equation 2, Appendix III), where a is the radius of the prolate spheroid top surface and h is the prolate spheroid height.

The fitting procedure was carried out by using software named "Prism 4". In this program, a parameter called fitting ratio 'R^2' served to measure quality of the fitting. Closeness of R^2 to a unity represents a measure of the fitting quality, where, ultimately, $R^2 = 1$ means perfect fit. The formula and fitting procedure are presented in Appendix III. The fitting results are shown in Table 7.

Table 7. Fitting results of glycerol/Rh:B FRAP experiments using Equation 1 (Appendix III)

Front surface*						
P_{pb} mW	**1×1 μm^2 D*10^{9}cm^2/s**	**1-R^2**	**1.1×1.1 μm^2 D*10^{-9}cm^2/s**	**1-R^2**	**1.26×1.26 μm^2 D*10^{-9}cm^2/s**	**1-R^2**
1	9.415	0.0874	3.891	0.0434	4.483	0.0489
2	4.170	0.0379	3.120	0.0169	3.639	0.0216
3	1.865	0.9779	3.002	0.0141	3.484	0.0188
Middle						
1	2.485	0.0721	3.132	0.1837	4.819	0.0367
2	2.334	0.0327	1.970	0.0255	1.804	0.0112
3	1.306	0.0158	1.745	0.0145	2.615	0.0124
Bottom surface						
1	2.057	0.0520	2.932	0.1158	2.720	0.0236
2	1.664	0.0190	2.852	0.0242	1.875	0.0116
3	1.391	0.0145	1.878	0.0143	1.565	0.0118

"1.P_{pb}=165 mW; 2. P_{pb}=331 mW; 3.P_{pb}=496 mW"

"Location of PBV in the sample, as described in Sub-Section 4.3.4"

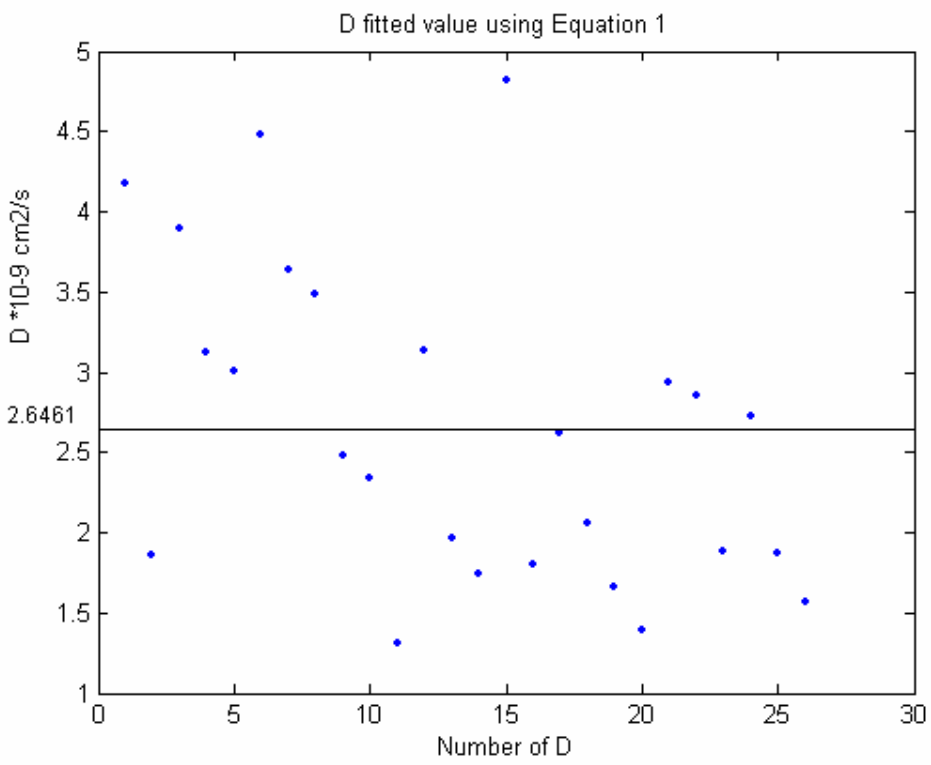

Fig 67. Diffusion coefficient *D* fitted with Equation 1 (FRAP in glycerol/Rh:B): the mean value was 2.6461×10^{-9} cm^2/s and the standard deviation was 0.9823×10^{-9} cm^2/s

From the results (see Table 7), it can be seen that all the fittings can be regarded as good fittings since the value of $1\text{-}R^2$ was sufficient small. Then, the FRAP data was fitted using the model, $a \neq h/2$ (see Table 8), and compared with these results.

Table 8. Fitting results of glycerol/Rh:B FRAP experiments using Equation 2 (Appendix III)

Front surface*						
P_{pb} mW	**1*1 μm^2 D*10^{9}cm^2/s**	**1-R^2**	**1.1*1.1μm^2 D*10^{-9}cm^2/s**	**1-R^2**	**1.26*1.26μm^2 D*10^{-9}cm^2/s**	**1-R^2**
1	11.122	0.0864	4.283	0.0399	4.516	0.0473
2	4.916	0.0372	3.448	0.0149	3.678	0.0202
3	2.245	0.0212	3.336	0.0121	3.545	0.0178
Middle						
1	2.964	0.0611	3.477	0.1834	4.852	0.0353
2	2.789	0.0313	2.220	0.0258	1.890	0.0110
3	1.590	0.0152	1.982	0.0140	2.690	0.0116
Bottom surface						
1	2.461	0.0516	3.256	0.1153	2.796	0.0227
2	2.005	0.0185	3.184	0.0236	1.968	0.0109
3	1.688	0.0137	2.131	0.0139	1.670	0.0111

"1.P_{pb}=165 mW; 2.P_{pb}=331 mW; 3.P_{pb}=496 mW"

"Location of PBV in the sample, as described in Sub-Section 4.3.4"

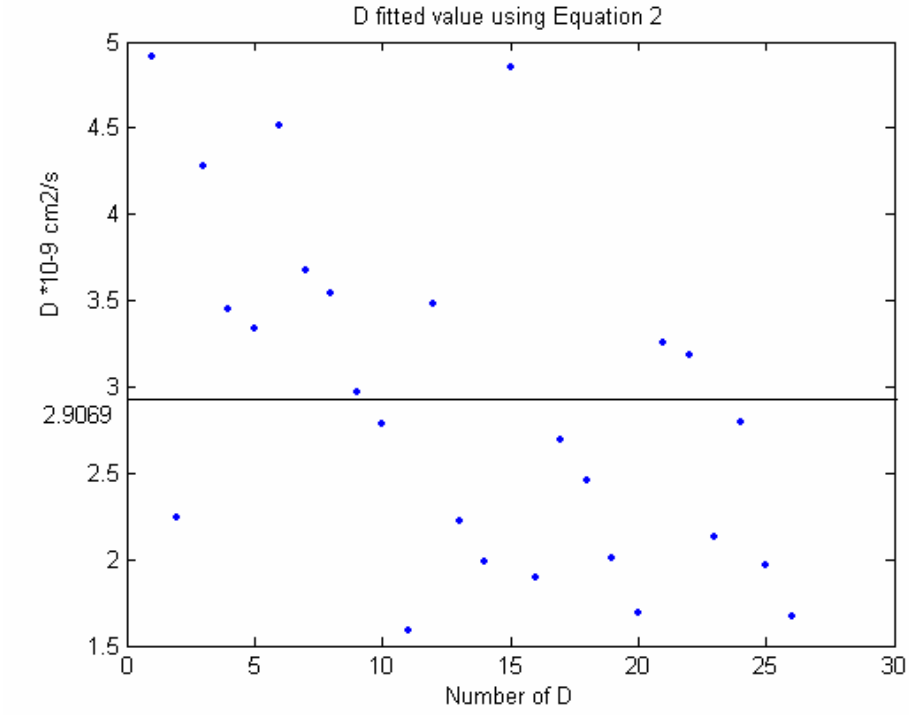

Fig 68. Diffusion coefficient *D* fitted with Equation 2 (FRAP in glycerol/Rh:B): the mean value was 2.9069 ×10^{-9} cm^2/s and the standard deviation was 0.9885×10^{-9} cm^2/s

Comparing of 1-R^2 values showed in Table 8 with those in Table 7, shows that the Equation 2 yields a little bit more accurate fitting results for getting smaller value of *1-R^2*. Nevertheless, the mean value of Equation 1 (2.6461×10^{-9} cm^2/s), was more near the calculated value (2.4×10^{-9} cm^2/s). Also, its standard deviation was smaller (0.9823×10^{-9} cm^2/s). In spite of these, there was not big difference for the values of *D* obtained from these two equations.

4.3.4 FRAP in *stratum corneum*

Since P_{pb} was found to have little influence on the FRAP process dynamics (from the previous measurement using the glycerol/Rh:B sample), P_{pb} = 165 mW was selected for FRAP experiments using skin. The higher P_{pb} could damage the skin. Also, a longer measurement time was required to attain the full recovery of the fluorescence signal, usually, from several minutes up to one hour. Similarly, it was resorted to use the smallest PBA (radius, 1 μm). Localisation is tighter, and the skin lipid bilayers were targeted more accurately. An example of the typical skin imaging layouts for FRAP measurement using P_{pb} = 165 mW are shown in Fig 69 and 70.

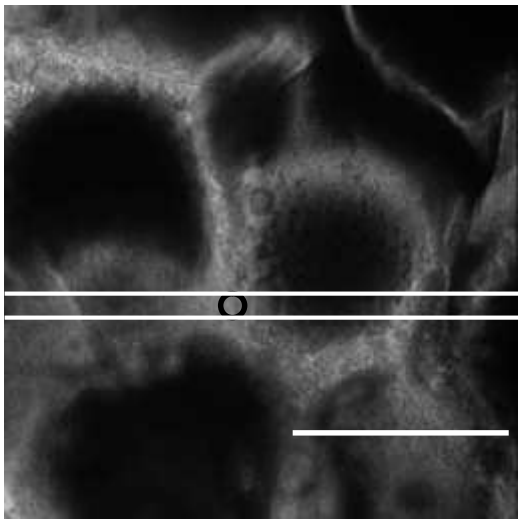

Fig 69. An FMM image of the excised skin showing clear layout of the bilipid layers in *stratum corneum*. A black circle marks where the PBA location. Linear dimension of PBA is 19 pixels (radius 1 μm). Scale bar 30 μm

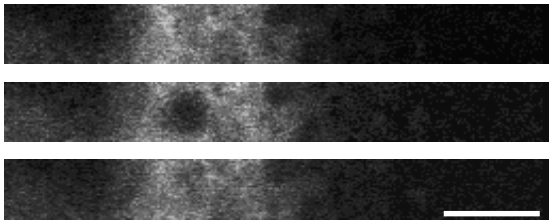

Fig 70. FRAP time-lapse images (the image fragment sampled within two white lines in Fig 67). From top to bottom: before, 282 ms after, and 8 s after photobleaching, respectively. Scale bar 5 μm

From these experiments, it was found that P_{sc} in skin (*stratum corneum*) distorted the recovery FRAP signal. As shown in Fig 71, the fluorescence recovery process competed with the photobleaching process induced by the probing femtosecond laser.

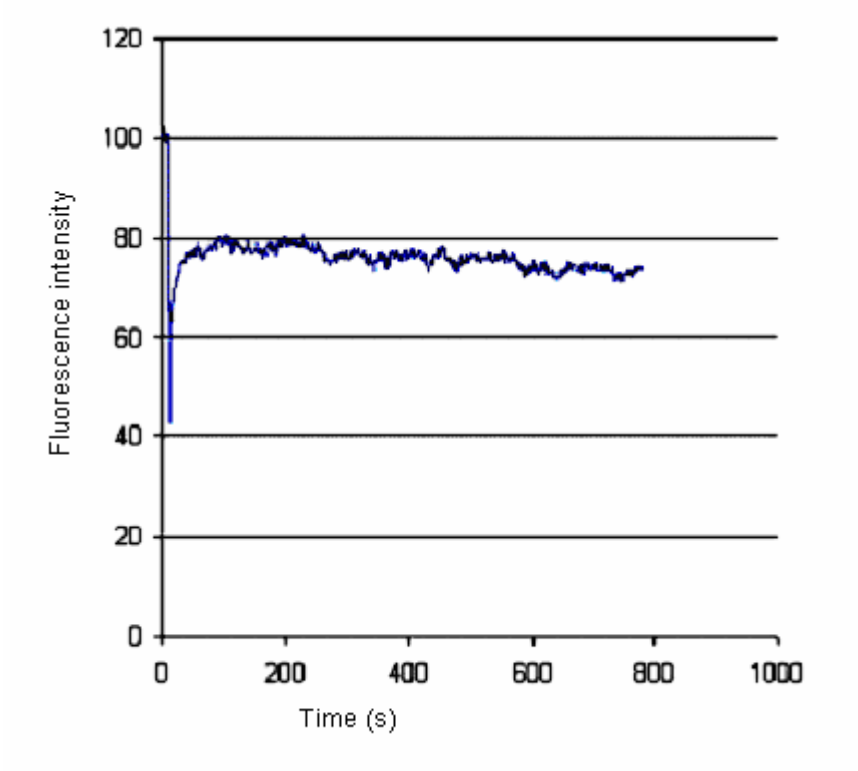

(a)

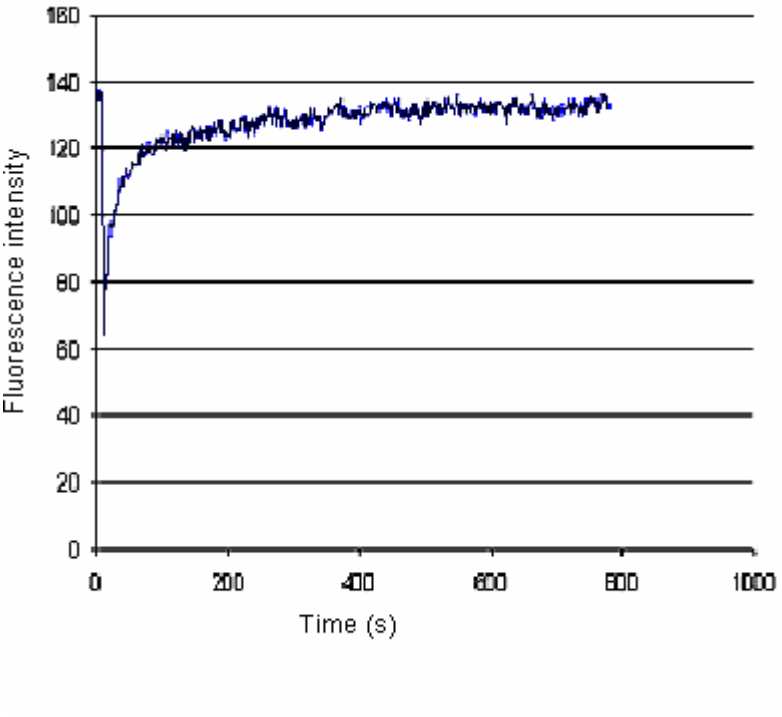

(b)

Fig 71. FRAP signal recording at two varied parameters: (a) P_{sc} = 33 mW; b) P_{sc} = 16.5 mW

From the curves of Fig 71, one can see that P_{sc} = 33 mW allows FRAP signal recovery of only 80% of that of the original value, whereas at P_{sc} = 16.5 mW, it recovered to 90% to its original value. Also, the FRAP signal exhibited further photobleaching t after recovery to 80% of the original intensity, as shown in Fig 71 (a). P_{sc} = 16.5 mW appeared to be the optimum value under the typical experimental conditions. The lower values of P_{sc} resulted in noisy FRAP signals.

For the preliminary FRAP experiments on the excised skin, P_{pb} = 165 mW, and P_{sc} = 16.5 mW were chosen. FRAP experiments in three layers of *stratum corneum* were carried out: top surface (1-2 μm from top), middle (10 μm to top) and bottom (20 μm to top). The results are shown in Fig 72 to Fig 74. Two types of PBAs were tried: circle and square, both were 19 pixels of equal linear dimensions of 2 μm. These experiments were only carried on stratum corneum but not limited to it. Epidermis is also a good research target to investigate. This will be the future aimed study.

Fig 72. FMM image of the excised skin, *stratum corneum* (top surface). The bleached area is marked by a black circle. Scale bar 30 μm

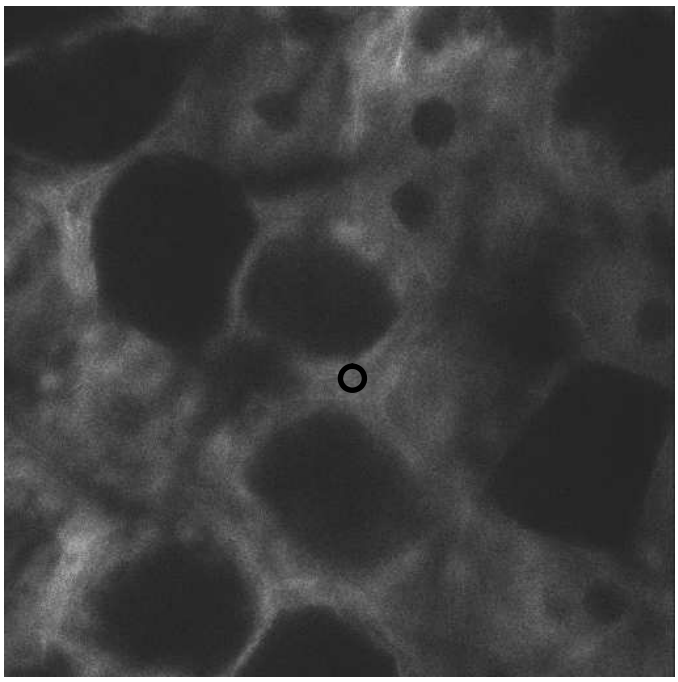

Fig 73. FMM image of the excised skin, *stratum corneum* (mid-depth). The bleached area is marked by a black circle. Scale bar 30 μm

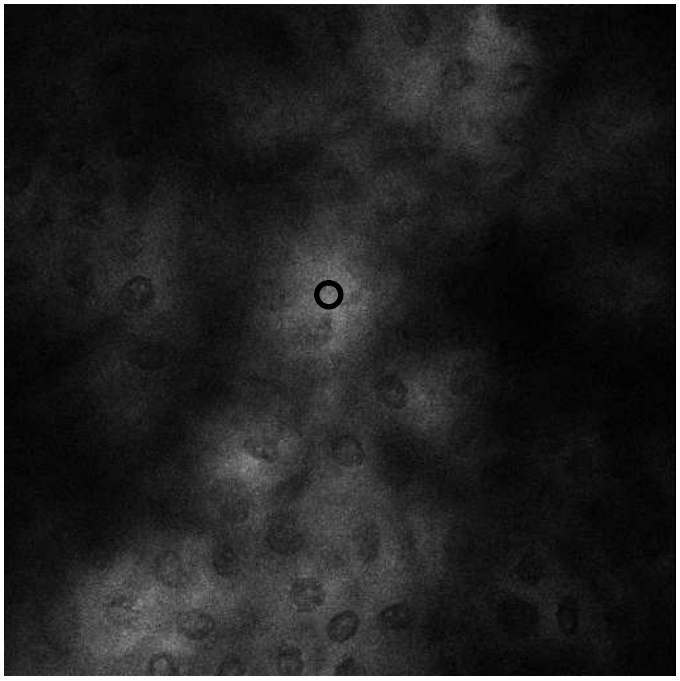

Fig 74. FMM image of the excised skin, *stratum granulosum*. Cells with dark nuclei are observable. The bleached area is marked by a black circle. Scale bar 30 μm

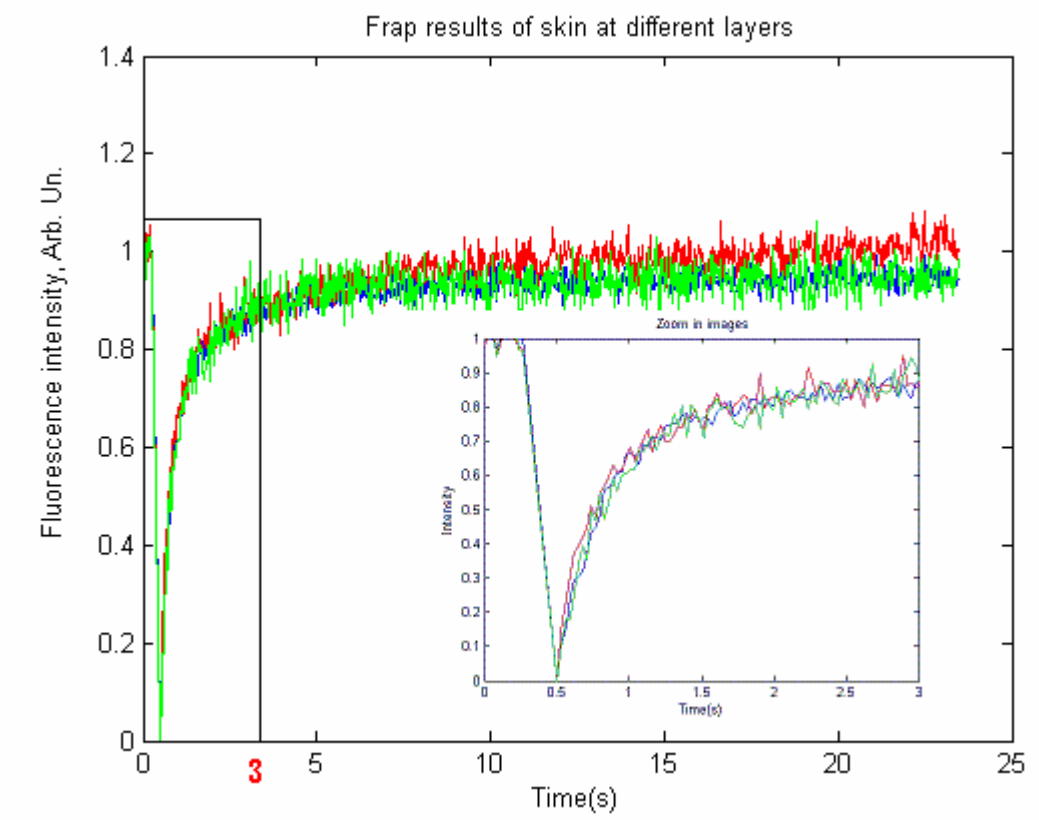

(a)

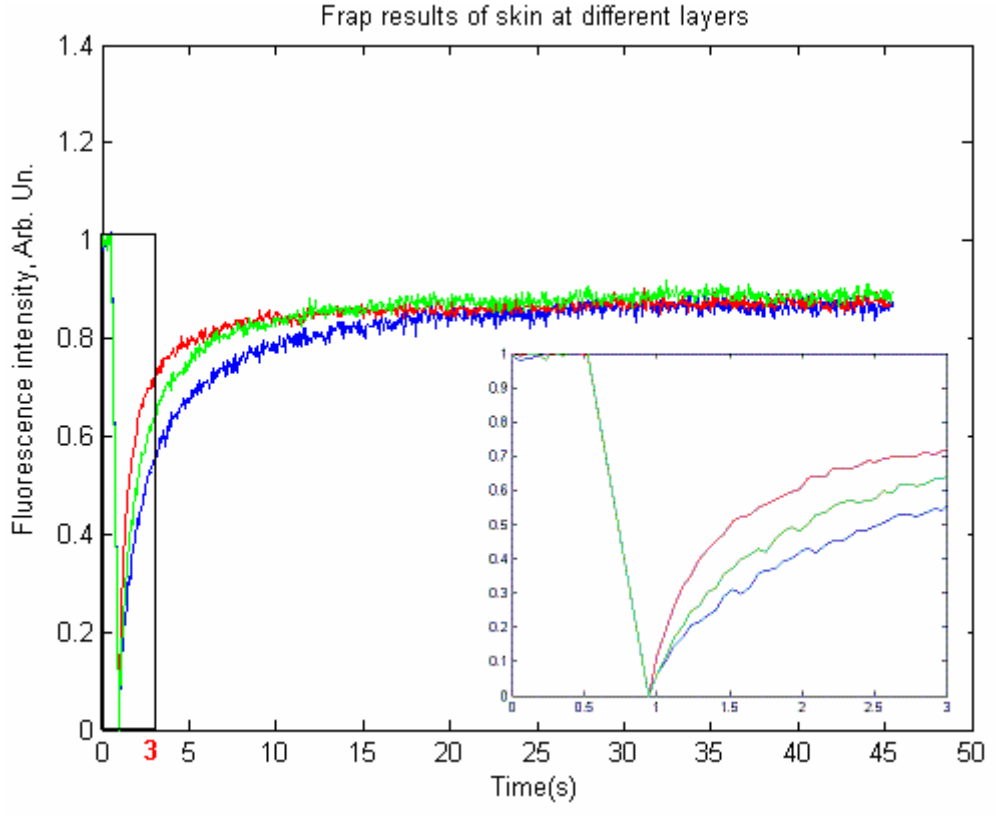

(b)

Fig 75. FRAP results of skin in the different *stratum corneum* layers: top surface, mid-depth, *stratum granulosum*, colour-coded blue, red, and green, respectively. The skin layer choice and depth values are given in Sub-Section 4.3.5. (a) PBA 1×1 μm^2 circular shape, (b) PBA 1×1 μm^2 square shape

From the normalised FRAP curves in Fig 75, especially from the insets (bottom right on the image), one can see that the recovery rate was similar at the different skin (*stratum corneum* /*stratum granulosum*) layers for the circular PBA. At the same time, the FRAP recovery rate exhibited difference at different localities in case of PBV of square cross-section. It showed that the fitting model based on the squire-cross-sectional PBV provided more accurate measurement of the diffusion coefficient at different sample sites in the skin.

Data fitting results

The prolate spheroid model was the same as that used in the glycerol/Rh:B fluorescent model experiments. The results of the fitting model based on cubic PBV were presented by Equations 3 and 4 ($a = h/2$ and $a \neq h/2$, Appendix III). The details of the fitting procedure are presented in Appendix III.

Table 9. Fitting results of skin (*stratum corneum*) FRAP experiments

Prolate spheroid model	$a = h/2$		$a \neq h/2$ (h=3 μm)	
	D *$\mathbf{10^{-9}}$ cm^2/s	$\mathbf{1}$-R^2	D*$\mathbf{10^{-9}}$ cm^2/s	$\mathbf{1}$-R^2
Top surface	5.598	0.0317	6.881	0.0306
Mid-depth	3.861	0.0617	4.792	0.0611
stratum granulosum	5.408	0.0874	6.548	0.0877
Cubic model	$a = h/2$		$a \neq h/2$ (h=3 μm)	
	D*$\mathbf{10^{-9}}$ cm^2/s	$\mathbf{1}$-R^2	D*$\mathbf{10^{-9}}$ cm^2/s	$\mathbf{1}$-R^2
Top surface	1.393	0.0049	1.734	0.0049
Mid-depth	3.625	0.0055	4.576	0.0054
stratum granulosum	2.031	0.0052	2.545	0.0051

"Location of PBV in the sample, as described in Sub-Section 4.3.5"

The fitting results in Table 9 for the diffusion coefficient determination in skin showed similar trend with that of the glycerol/Rh:B model: the fitting model $a \neq h/2$ provided more accurate fitting results than $a = h/2$, as measured by the 1-R^2 values. The fitting model did not consider the boundary effects and therefore the fitting results in the mid-depth of *stratum corneum* were more reasonable. Thus, the D–values in skin were represented by the values in the mid-depth layer. The D-values of the two models were approximately $4.3\times10^{-9} \pm 0.6583$ cm^2/s (prolate spheroid PBV) and $4.1\times10^{-9} \pm 0.6725$ cm^2/s (cubic PBV).

4.4 Discussion

The prolate spheroid PBV FRAP model was based on the theory which was presented by Braeckmans et al. (Braeckmans, 2003). The cubic PBV FRAP model is a generalisation of the prolate spheroid PBV FRAP model, with the square PBA. All the fittings were good fit measured by $1\text{-}R^2$. The values of *D*s were on the same scale of the estimated value but still had some difference. There are several reasons for this discrepancy. Firstly, the boundary effects in the diffusion model should be considered, when modelling the FRAP signal near the sample interface. In the simplified model, these effects were neglected. Secondly, the temperature at PBV might increase, as a result of the laser energy dissipation in the absorptive parts of the sample. The resultant *D*, that depends on temperature, might yield the overestimated values of *D*, as was pointed out in case of the varied viscosity of glycerol that changed with the temperature (Cook, 1994). Since it was difficult to sample local temperature at the interrogated PBV, this potential disturbing effect might introduce a systematic error in the measurements. Thirdly, the FRAP data fitting quality depended on the choice of fitting prolate spheroid model. In case of $a = h/2$, this model yielded more accurate fitting results. That implies that the choice of PBD was critical to the quality of the FRAP data fitting. At the same time, the choice of PBD was not reliable, as it highly varied with the location of PBV in the sample (see Fig 63). Therefore, it needed to figure out an efficient and reliable method setting PBD.

FRAP-based determination of *D* in heterogeneous tissue, including skin, has been extensively addressed in literature. Brown have reported *D* of Red Blood (RBL)-2H3cells in inaqueous solutions of wild-type green fluorescent protein, which was measured as 8.7×10^{-7} cm^2/s using FMM FRAP (Brown, 1999). Leddy and Guilak have demonstrated determination of *D* of macromolecules in the cartilage the using FRAP-FCSM technique, which was found to range from 31 to 75 $\times10^{-8}$ cm^2/s versus molecule weights (Leddy and Guilak, 2003). Also, Sniekers has reported D = 5.22 - 25 $\times10^{-8}$ cm^2/s in cartilaginous tissue. They have demonstrated a new method called finite element analysis using FCSM (Sniekers and van Donkelaar, 2005). Recently, Johnson and his colleagues have published *D* = 3.06 - 23.4 $\times10^{-9}$ cm^2/s depending on the molecule weight of the extracted lipid bilayers. The used FCSM imaging modality performed FRAP, with PBA restricted to 5 μm (Johnson, 1996). With this backdrop, the FRAP results on determination of *D* in human skin lipid bilayers are reported first time to the best of the knowledge. Compare to Johnson's results, *D* of Rh:B in the stratum corneum was $\backsimeq 4\times10^{-9}$ cm^2/s that was within the range of *D* of 3.06 - 23.4 $\times10^{-9}$ cm^2/s. The molecule

weight was ranged from 223 to 854 Da in the Johnson's paper. The molecule weight of Rh:B is 479 Da, which is in the same range. Therefore, diffusion coefficient within *stratum corneum* was confirmed with the results obtained from the extracted lipid bilayers. The results using FMM imaging modality integrated with FRAP methodology were obtained, whereas Johnson has used FCSM that conferred several disadvantages, such as the out-of-focus photobleaching. Also, in the method, it was succeeded in decreasing of PBA to 1 μm in the linear dimension that was advantageous in providing finer localisation of FRAP signal (and *D*) sampling of lipid bilayers that are on the scale of 1 - 2 μm. In addition, Scheuplein has reported the intracellular *D* of 1 - 10×10^{-11} cm^2/s in dry skin and 5 - 10×10^{-10} cm^2/s in wet skin by measuring steady-state flux of solute, the change of solute concentration within skin (Scheuplein, 1971). Compare to these values, *D* obtained in *stratum corneum* appeared to be much greater which was (4×10^{-9} cm^2/s) implying the diffusion dynamics much faster that that reported by Scheuplein. This brings about a reasonable hypothesis that the diffusion within *stratum corneum* predominantly occurs via intercellular pathways whereby molecular diffusion rate is known to be much faster to that of the intracellular biological pathway, i.e. via corneocytes.

4.5 Conclusion

Application of the FRAP technique implemented in FMM imaging modality was demonstrated to determine diffusion coefficient in *stratum corneum*. It has been found D $=4\times10^{-9}$ cm^2/s in *stratum corneum* was confirmed by the results obtained in the extracted lipid bilayers by Johnson. Compared to *D* obtained in intracellular pathways (through corneocytes) of 10^{-11} - 10^{-9} cm^2/s, the value of *D* was much greater. It had a reasonable explanation of the diffusion process predominantly occurring through lipid bilayers at a considerably faster rate.

There are also many other research points in this project for future study. Firstly, the skin FRAP experiments were mainly carried out in *stratum corneum*. However, epidermis represents a skin layer of great interest, as the first topmost viable layer of the human body. The diffusion mechanism within this layer provides important information on the drug pharmakodynamics and pharmakinetics. Secondly, the *stratum corneum* heterogeneity calls for much more extensive study of *D* in *stratum corneum* at different skin sites, including abdomen, back, arm. Also, *D*-maps of skin of different types of skin (age, ethics, and gender) will provide valuable information on the skin transdermal permeability properties versus genotype. These problems represent potentially important prospective research topics. Thirdly,

other fluorescent agents, especially of broadly variable molecular weight, should be thoroughly investigated. The list of exogenous fluorophores includes fluorescein, Rhodamine-ester, and nanometre-scale luminescent nanoparticles. Also, Rh:B has an undesirable protein affinity property that may introduce uncontrollable artefacts in the recover process. Rh:B-Ester is a good replacement candidate for carrying out further research to investigate the bounding effects of skin.

Chapter 5 Conclusion

Nowadays, investigation of the skin biological pathways is an important research topic. This research project has been focused on investigation of nanoparticle transdermal penetrability by applying the advanced optical microscopes, including FMM. The second focus of this thesis was on study of transdermal transport, where organic dye served as a model of transported solute by theoretical and experimental modelling of diffusion in skin (*stratum corneum*).

Nanoparticles penetration within skin is important from the environmental toxicology and drug delivery aspects. Not all mechanisms of nanoparticle transdermal penetrability are well understood, and some are hotly debated. It is generally agreed that the nanoparticle size represents the key parameter that determines the nanoparticle penetrability through skin. At the same time, the nanoparticle size threshold is hypothesised but not corroborated experimentally yet. In the study, nanoparticles of three types, ZnO-nano, TiO_2-nano, and Qdots that ranged in size from 14 to 35 nm were focused on, and investigated their penetrability in skin under various conditions and skin treatments. The main findings are the following:

1. The nanoparticles of the reported size range do not pass the *stratum corneum* layer of intact human skin, and remain in skin folds, derma glyphs, and hair follicle shafts.
2. It is for the first time, nanoparticle penetrability has been tested in skin *in vivo* using serendipitous optical properties of ZnO-nano, and confirmed the major verdict of the *in vitro* studies – the nanoparticle negative uptake.
3. The nanoparticle surface modification, the skin physical treatment, including flexing and stretching, make little effect on the found negative uptake of the nanoparticle by skin.
4. *Stratum corneum* provides the main barrier against the environmental insult in form of nanoparticle absorption in the viable layers of skin. The removal of this barrier results in the dramatic enhancement of the transdermal penetrability.
5. Porcine skin provides a poor model of human skin in the context of nanoparticle transdermal penetrability. Qdots of the investigated size range are generally taken by the porcine skin, where the uptake rate and nanoparticle fate depends on various parameters.

6. The chemical enhancers have dramatic effects on skin, and render it considerably more penetrable. These effects were conclusively confirmed by using FMM and SEM/EDS.

The demonstration of application of FRAP technique to determination of dye diffusion coefficient locally, has resulted in the following outcomes:

1. A new FRAP modality integrated into the FMM system has been introduced.
2. The existing diffusion model in the framework of FRAP was refined, and found that modelling the PBV as an prolate spheroid or square-cross-section ellipsoid give the most accurate fitting results from which *D* can be accurately determined.
3. D of Rh:B within *stratum corneum* was determined that was valued as 4×10^{-9} cm^2/s. This result was in agreement with *D* of the extracted lipid bilayers.

Publications

1. **X. Zhao**, A. Gierden, J. A. Ross, M. Sarkar, W. Sanchez, A. V. Zvyagin, M. S. Roberts, "Nanoparticles penetration through human skin, Much ado about nothing?", "*Trailblazing the Skin Frontier: Evidence Base, Opportunities&Training*", George Washington University, Washington, D.C., 11-13 August, 2007.
2. **X. Zhao**, J. A. Ros, M. Sakar, M. S. Roberts, A. V. Zvyagin, "Application of Multiphoton Microscopy to Study of Nanoparticle Penetration through Skin *in vitr*o and *in vivo*", *3rd Asian and Pacific Rim Symposium on Biophotonics APBP2007 & Biophotonics Down Under II*, July, 2007, "Program&Book of Abstracts", p. 118 , 2007.
3. **X. Zhao**, A. V. Zvyagin, Y. Anissimov, M. S. Roberts, "The use of multiphoton microscopy for assessment of absorption of selected chemicals in skin", *Annual Seminar of Fluorescence Applications in Biotechnology and Life Sciences (FABLS)*, Coffs Harbour, October, 2006.
4. Michael Roberts**, Xin Zhao,** Washington Sanchez**, "**Multiphoton imaging of zinc oxide nanoparticle penetration into human skin *in vivo* and *in vitro*", *2nd Advanced Optical Imaging Workshop*, The university of Melbourne, Australia, November 26-28, 2007.
5. A. V. Zvyagin, **X. Zhao**, W. Sanchez, J. A. Ross, M. S. Roberts, "Optical Imaging of Nanoparticle Penetration in Human Skin *in vitro* and *in vivo*", *International Conference on Laser Applications in Life Sciences*, Taiwan, 4-6 December, 2008.
6. A. V. Zvyagin, **X. Zhao**, W. Sanchez, J. A. Ross, M. S. Roberts, "Optical Imaging of Nanoparticle Penetration in Human Skin *in vitro* and *in vivo*", *Australian Institute of Physics (AIP) 18th National Congress*, Adelaide, South Australia, 30 November - 5 December, 2008.
7. Andrei V. Zvyagin, **Xin Zhao**, "Imaging of Zinc Oxide Nanoparticle Penetration in Human Skin *in vitro* and *in vivo*", accepted by Journal of Biomedical Optics, 2008, Manuscript ID: JBO 08185R.
8. Roberts M., **Zhao X.**, "*In vitro* and *in vivo* imaging of xenobiotic transport in human skin and in the rat liver", accepted by Journal of Biophotonics, 2008, Manuscript ID: JBIO-2008-00058.R1.

Reference

Adams, L. K. (2006). "Comparative eco-toxicity of nanoscale TiO_2, SiO_2, and ZnO water suspensions". Water Research 40(19): 3527-3532.

Alvarez-Roman, R., A. Naik, et al. (2004). "Skin penetration and distribution of polymeric nanoparticles." Journal of Controlled Release 99(1): 53-62.

B.R. Masters (1998). "Optical Biopsy of *In vivo* Human Skin: Multi-photon Excitation Microscopy." Lasers in Medical Science 13(3): 196-203.

Bahnemann, D. W., C. Kormann, et al. (1987). "Preparation and Characterization of Quantum Size Zinc-Oxide - a Detailed Spectroscopic Study." Journal of Physical Chemistry 91(14): 3789-3798.

Baker, H. (1967). "Measurement of transepidermis water loss by electrical hygrometry." Arch. Dermatol. 96: 441-452.

Baroli, B., M. G. Ennas, et al. (2007). "Penetration of metallic nanoparticles in human full-thickness skin." Journal of Investigative Dermatology 127(7): 1701-1712.

Barry, B. W. (2001). "Novel mechanisms and devices to enable successful transdermal drug delivery." European Journal of Pharmaceutical Sciences 14(2): 101-114.

Bauer, R. K., P. d. Mayo, et al. (1982). "Surface Photochemistry. The Photophysics of Pyrene Adsorbed on Silica Gel, Alumina,and Calcium Fluoride." J. Phys. Chem. 86: 3781-3789.

Becker, W. (2006). "Fluorescence Lifetime Imaging by Multi-Dimensional TCSPC, A Multi-Spectral FLIM Technique for Laser Scanning Microscope."

Beduneau, A., P. Saulnier, et al. (2007). "Active targeting of brain tumours using nanocarriers". Biomaterials 28(33): 4947-4967.

Bemporad, D., C. Luttmann, et al. (2004). "Computer simulation of small molecule permeation across a lipid bilayer: Dependence on bilayer properties and solute volume, size, and cross-sectional area." Biophysical Journal 87(1): 1-13.

Benson, H. A. (2005). "Transdermal drug delivery: penetration enhancement techniques." Curr Drug Deliv 2(1): 23-33.

Booth, M., M. Neil, et al. (2002). "Adaptive aberration correction in a confocal microscope." Proceedings of the national academy of sciences of the United States of America 99(9): 5788-5792.

Braeckmans, K., L. Peeters, et al. (2003). "Three-dimensional fluorescence recovery after photobleaching with the confocal scanning laser microscope." Biophys J 85(4): 2240-2252.

Braga, J., J. M. P. Desterro, et al. (2004). "Intracellular macromolecular mobility measured by fluorescence recovery after photobleaching with confocal laser scanning microscopes." Molecular Biology of the Cell 15(10): 4749-4760.

Braginsky, L. and V. Shklover (1999). "Light absorption in TiO_2 nanoparticles". European Physical Journal D 9(1-4): 627-630.

Brauer, G., J. Kuriplach, et al. (2007). "Positron lifetimes in ZnO single crystals." Vacuum 81(10): 1314-1317.

Brown, E. B., E. S. Wu, et al. (1999). "Measurement of molecular diffusion in solution by multiphoton fluorescence photobleaching recovery." Biophys J. 77(5): 2837-2849.

Burch, G. E. (1946). "Rate of insensible perspiration locally through living and dead human skin." Arch. Internal Med. 74: 437-444.

Buzea, C., Pacheco, II, et al. (2007). "Nanomaterials and nanoparticles: Sources and toxicity". Biointerphases 2(4): MR17-MR71.

Chang, E., N. Thekkek, et al. (2006). "Evaluation of quantum dot cytotoxicity based on intracellular uptake." Small 2(12): 1412-1417.

Cheng, H. M., H. Cheng, et al. (2005). "Efficient UV photoluminescence from monodispersed secondary ZnO colloidal spheres synthesized by sol–gel method " Journal of Crystal Growth 277: 192.

Cheng, H. M., K. F. Lin, et al. (2006). "Size dependence of photoluminescence and resonant Raman scattering from ZnO quantum dots." Applied Physics Letters 88(26).

Cole, L. and C. Heard (2007). "Skin permeation enhancement potential of Aloe Vera and a proposed mechanism of action based upon size exclusion and pull effect." Int J Pharm 333(1-2): 10-16.

Cook, R. L., H. E. King, et al. (1994). "Pressure and temperature dependent viscosity of two glass forming liquids: Glycerol and dibutylphthalate." J.Chem.Phys 100(7): 5178-5189.

Cross, S. E., B. Innes, et al. (2007). "Human skin penetration of sunscreen nanoparticles: in-vitro assessment of a novel micronized zinc oxide formulation." Skin Pharmacol Physiol 20(3): 148-154.

Cox, I. J., C. J. R. Sheppard, et al. (1982). "Super-resolution by confocal fluorescent microscopy." OPTIK 60(4): 391-396.

Dalton, C. H., I. J. Hattersley, et al. (2006). "Absorption of the nerve agent VX (O-ethyl-S-[2(di-isopropylamino)ethyl] methyl phosphonothioate) through pig, human and guinea pig skin *in vitro*." Toxicology *in Vitro* 20(8): 1532-1536.

Demir, M. M., R. Munoz-Espi, et al. (2006). "Precipitation of monodisperse ZnO nanocrystals via acid-catalysed esterification of zinc acetate". Journal of Materials Chemistry 16(28): 2940-2947.

Denk, W. (1997). "Multiphoton microscopy: Imaging with nonlinear optics." Photonics spectra 31(7): 125-+.

Denk, W. and K. Svoboda (1997). "Photon upmanship: Why multiphoton imaging is more than a gimmick." Neuron 10(3): 351-357.

Dietz, G. P. H. and M. Bahr (2004). "Delivery of bioactive molecules into the cell: The Trojan horse approach". Molecular and Cellular Neuroscience 27(2): 85-131.

Dong, G., Zheng, Y., Yi-Bo, et al. (2005). "Photoluminescence mechanism of ZnO:Zn investigated by microwave dielectric spectrometry". Chin.Phys.Lett. 22(8): 2092-2095.

Dong, W. (2004). Monitoring chemically enhanced transdermal delivery pathways of luminescent quantum dots by multiphoton microscopy. Biophotonics, APBP 2004. The Second Asian and Pacific Rim Symposium on.

Draper, R. B. and M. A. Fox (1990). "Titanium Dioxide Photosensitized Reactions Studied by Diffuse Reflectance Flash Photolysis in Aqueous Suspensions of TiO_2 Powder". Langmuir 6: 1396-1402.

Duan, H. W. and S. M. Nie (2007). "Cell-penetrating quantum dots based on multivalent and endosome-disrupting surface coatings." Journal of the American Chemical Society 129(11): 3333-3338.

Dunford, R., A. Salinaro, et al. (1997). "Chemical oxidation and DNA damage catalysed by inorganic sunscreen ingredients". Febs Lett 418(1-2): 87-90.

Eisinger, J., J. Flores, et al. (1986). "A milling crowd model for local and long-range obstructed lateral diffusion. Mobility of excimeric probes in the membrane of intact erythrocytes". Biophys J 49(5): 987-1001.

Evgenidou, E., I. Konstantinou, et al. (2007). "Photocatalytic oxidation of methyl parathion over TiO_2 and ZnO suspensions". Catalysis Today 124(3-4): 156-162.

Fu, S. and Chia, T. C., et al. (2001). "Study of laser induced normal human skin *in vivo* autofluorescence spectra." Proceedings of SPIE, Diagnostic optical spectroscopy in biomedicine 4432: 230-235.

Fujishima, A. and K. Honda (1972). "Electrochemical Photolysis of Water at a Semiconductor Electrode". Nature 238: 37-38.

Gamer, A. O., E. Leibold, et al. (2006). "The *in vitro* absorption of microfine zinc oxide and titanium dioxide through porcine skin." Toxicology *in Vitro* 20: 301-307.

Gan, X., G. Min, et al. (1992). "Fluorescent image-formation in the fiberoptic confocal scanning microscope." Journal of modern optics 39(4): 825-834.

Genina, E. A., A. N. Bashkatov, et al. (2002). "*In vitro* and *in vivo* study of dye diffusion into the human skin and hair follicles." Journal of Biomedical Optics 7(3): 471-477.

Gopee, N. V., D. W. Roberts, et al. (2007). "Migration of intradermally injected quantum dots to sentinel organs in mice". Toxicological sciences 98(1): 249-257.

Hanson, K. M., M. J. Behne, et al. (2002). "Two-photon fluorescence lifetime imaging of the skin straum corneum pH Gradient". Biophysical Journal 83: 1682-1690.

Hariharan, C. (2006). "Photocatalytic degradation of organic contaminants in water by ZnO nanoparticles: Revisited". Applied Catalysis A: General 304: 55-61.

Harvey, H. (2000). "Autofluorescence properties of skin and applications in dermatology." Proceedings of SPIE, the International Society for Optical Engineering 4224: 366-373.

Hayden, C. G., S. E. Cross, et al. (2005). "Sunscreen penetration of human skin and related keratinocyte toxicity after topical application." Skin Pharmacol Physiol 18(4): 170-174.

Helmchen, F. and W. Denk (2005). "Deep tissue two-photon microscopy." Nature Methos 2(12): 932-940.

Honda, C., Y. Katsumata, et al. (2006). "Temperature dependence of pyrene fluorescence spectra in aqueous solutions of CnEm (C14E7, C16E7, and C16E6) nonionic surfactant micelles." Journal of Photochemistry and Photobiology a-Chemistry 182(2): 151-157.

Invitrogen The future of fluorescence, Invitrogen.

Ipe, B. I., M. Lehnig, et al. (2005). "On the generation of free radical species from quantum dots." Small 1(7): 706-709.

Irimpan, L., V. P. N. Nampoori, et al. (2008). "Size-dependent enhancement of nonlinear optical properties in nanocolloids of ZnO". Journal of Applied Physics 103(3).

Jacobi, U., M. Kaiser, et al. (2007). "Porcine ear skin: an *in vitro* model for human skin." Skin Res Technol 13(1): 19-24.

Jacobi, U., R. Toll, et al. (2005). "Do follicles play a role as penetration pathways in *in vitro* studies on porcine skin?-An Optical Study." Laser Physics 15(11): 1594-1598.

Jeng, H. A. and J. Swanson (2006). "Toxicity of metal oxide nanoparticles in mammalian cells." Journal of Environmental Science and Health Part a-Toxic/Hazardous Substances & Environmental Engineering 41(12): 2699-2711.

Jin, X. and Y. Kusumoto (2003). "Spectroscopic studies of pyrene adsorbed to titanium dioxide." Chemical Physics Letters 378: 192-194.

Johnson, M. E., D. A. Berk, et al. (1996). "Lateral diffusion of small compounds in human stratum corneum and model lipid bilayer systems." Biophysical Journal 71(5): 2656-2668.

Johnson, M. E., D. Blankschtein, et al. (1997). "Evaluation of solute permeation through the stratum corneum: Lateral bilayer diffusion as the primary transport mechanism." Journal of Pharmaceutical Sciences 86(10): 1162-1172.

Jung, S., N. Otberg, et al. (2006). "Innovative liposomes as a transfollicular drug delivery system: penetration into porcine hair follicles." J Invest Dermatol 126(8): 1728-1732.

Kaufman, G., B. A. Horwitz, et al. (2007). "Infection stages of the dermatophyte pathogen Trichophyton: microscopic characterization and proteolytic enzymes." Medical Mycology 45(2): 149-155.

Kendall, M., T. Mitchell, et al. (2004). "Intradermal ballistic delivery of micro-particles into excised human skin for pharmaceutical applications." Journal of Biomechanics 37(11): 1733-1741.

Kimura, S. and T. Wilson (1993). "Effect of axial pinhole displacement in confocal microscopes." Applied Optics 32(13): 2257-2261.

Kollias, N., R. Gillies, et al. (1998). "Endogenous skin fluorescence includes bands that may serve as quantitative markers of aging and photoaging". Journal of Investigative Dermatology 111(5): 776-780.

König, K., Ehlers, et al. (2006). "Multiphoton tomography of skin and nanoprocessing with near infrared femtsecond laser pulses, Fraunhofer Institute of Biomedical Technology (IBMT)", St. Ingbert, Germany, Dept. of Dermatology and Allergology, Friedrich Schiller University, Jena: 47.

König, K., A. Ehlers, et al. (2006). "*In vivo* drug screening in human skin using femtosecond laser multiphoton tomography ". Skin Pharmacol Physi 19(2): 78-88.

Lademann, J., H. Richter, et al. (2006). "Hair follicles - A long-term reservoir for drug delivery." Skin Pharmacology and Physiology 19(4): 232-236.

Laiho, L. H., S. Pelet, et al. (2005). "Two-photon 3-D mapping of ex vivo human skin endogenous fluorescence species based on fluorescence emission spectra." J Biomed Opt 10(2): 024016.

Laiho, L. (2005). "Tissue imaging based on two-photon autofluorescence and second harmonic generation", The second joint EMBS/BMES Conference Houston.

Larson, D. R., W. R. Zipfel, et al. (2003). "Water-soluble quantum dots for multiphoton fluorescence imaging *in vivo* ". Science 300(5624): 1434-1436.

Lauer, A. C., C. Ramachandran, et al. (1996). "Targeted delivery to the pilosebaceous unit via liposomes." Advanced Drug Delivery Reviews 18(3): 311-324.

Leddy, H. A. and F. Guilak (2003). "Site-specific molecular diffusion in articular cartilage measured using fluorescence recovery after photobleaching." Annals of Biomedical Engineering 31: 753-760.

Lee, J. H., E. R. Carraway, et al. (2007). "Pyrene fluorescence in the presence of nonquenching and dynamic quenching salting-out agents." Journal of Photochemistry and Photobiology a-Chemistry 185(1): 57-61.

Lei, T. G., H. H. Bo, et al. (2005). "Effect of Microstructure of TiO_2 Thin Films on Optical Band Gap Energy". Chinese Phys. Lett. 22 1787-1789.

Li, Y., T. J. White, et al. (2004). "Low-temperature synthesis and microstructural control of titania nano-particles". Journal of Solid State Chemistry 177(4-5): 1372-1381.

Lide, D. R. (1992-1993). CRC handbook of chemistry and physics, 73rd edition.

Lin, K. F., H. M. Cheng, et al. (2005). "Band gap variation of size-controlled ZnO quantum dots synthesized by sol-gel method". Chemical Physics Letters 409(4-6): 208-211.

Linsebigler, A. L., G. Q. Lu, et al. (1995). "Photocatalysis on TiO_2 surfaces-principles, mechanisms, and selected results". Chemical Reviews 95(3): 735-758.

Lopez-Cervantes, M., E. Marquez-Mejia, et al. (2006). "Chemical enhancers for the absorption of substances through the skin: Laurocapram and its derivatives." Drug Dev Ind Pharm 32(3): 267-286.

Mak, V. H. W., R. O. Potts, et al. (1990). "Percutaneous penetration enhancement *in vivo* measured by attenuated total reflectance infrared spectroscopy." Pharmaceutical Research 7(8): 835-841.

Masters, B. R., P. T. C. So, et al. (1997). "Multiphoton excitation fluorescence microscopy and spectroscopy of *in vivo* human skin." Biophysical Journal 72(6): 2405-2412.

McNeil, S. E. (2005). "Nanotechnology for the biologist." J Leukoc Biol 78(3): 585-594.

Meidan, V. M., M. C. Bonner, et al. (2005). "Transfollicular drug delivery--is it a reality?" Int J Pharm 306(1-2): 1-14.

Mitragotri, S., M. E. Johnson, et al. (1999). "An analysis of the size selectivity of solute partitioning, diffusion, and permeation across lipid bilayers." Biophysical Journal 77(3): 1268-1283.

Monticone, S., R. Tufeu, et al. (1998). "Complex nature of the UV and visible fluorescence of Colloidal ZnO nanoparticles." Journal of Physical Chemistry B 102(16): 2854-2862.

Muth, J. F., R. M. Kolbas, et al. (1999). "Excitonic structure and absorption coefficient measurements of ZnO single crystal epitaxial films deposited by pulsed laser deposition". Journal of Applied Physics 85(11): 7884-7887.

Na, R., I. M. Stender, et al. (2001). "Autofluorescence of human skin is age-related after correction for skin pigmentation and redness." J Invest Dermatol 116(4): 536-540.

Na, R., I. M. Stender, et al. (2000). "Autofluorescence spectrum of skin: component bands and body site variations." Skin Res Technol 6(3): 112-117.

Narishetty, S. T. and R. Panchagnula (2005). "Effect of L-menthol and 1,8-cineole on phase behaviour and molecular organization of SC lipids and skin permeation of zidovudine." J Control Release 102(1): 59-70.

Nohynek, G. J., J. Lademann, et al. (2007). "Grey goo on the skin? Nanotechnology, cosmetic and sunscreen safety." Crit Rev Toxicol 37(3): 251-277.

Norlen, L. and A. Al-Amoudi (2004). "Stratum corneum keratin structure, function, and formation: the cubic rod-packing and membrane templating model." J Invest Dermatol 123(4): 715-732.

Oberdorster, G., E. Oberdorster, et al. (2005). "Nanotoxicology: An emerging discipline evolving from studies of ultrafine particles." Environmental Health Perspectives 113(7): 823-839.

Palero, J. A., H. S. d. Brujin, et al. (2007). "Spectrally resolved multiphoton imaging of *in vivo* and excised mouse skin tissue". Biophysical Journal 93(3): 992-1007.

Palik, E. D., Ed. (1985). Handbook of Optical Constants of Solids. London, Academic Press.

Pan, D. C., N. N. Zhao, et al. (2005). "Facile synthesis and characterization of luminescent TiO_2 nanocrystals". Advanced Materials 17(16): 1991-+.

Pan, Z. W., Z. R. Dai, et al. (2001). "Nanobelts of semiconducting oxides". Science 291(5510): 1947-1949.

Perez-Cullell, N., L. Coderch, et al. (2000). "Influence of the fluidity of liposome compositions on percutaneous absorption." Drug Deliv 7(1): 7-13.

Pflucker, F., V. Wendel, et al. (2001). "The human stratum corneum layer: An effective barrier against dermal uptake of different forms of topically applied micronized titanium dioxide." Skin Pharmacology and Applied Skin Physiology 14: 92-97.

Pinnell, S. R., D. Fairhurst, et al. (2000). "Microfine zinc oxide is a superior sunscreen ingredient to microfine titanium dioxide". Dermatologic Surgery 26(4): 309-313.

Rehn, B., F. Seiler, et al. (2003). "Investigations on the inflammatory and genotoxic lung effects of two types of titanium dioxide: untreated and surface treated". Toxicology and Applied Pharmacology 189(2): 84-95.

Roberts, M. (2006). United States of Ameraca Department of Health and Human Services, Food and Drug Administration Nanotechnology Task Force Public Meeting on Nanotechnology Materials in FDA Regulated Products, National Institutes of Health, Bethesda, MD.

Rouse, J. G., J. Z. Yang, et al. (2007). "Effects of mechanical flexion on the penetration of fullerene amino Carboxylic-derivatized peptide nanoparticles through skin." Nano Letters 7(1): 155-160.

Ryman-Rasmussen, J. P., J. E. Riviere, et al. (2006). "Penetration of intact skin by quantum dots with diverse physicochemical properties." Toxicol Sci 91(1): 159-165.

Ryman-Rasmussen, J. P., J. E. Riviere, et al. (2007). "Surface coatings determine cytotoxicity and irritation potential of quantum dot nanoparticles in epidermal keratinocytes." Journal of Investigative Dermatology 127(1): 143-153.

Sanchez, W. H. (2005). "Elucidating the role of silicone in the treatment of burn scars: an essential step in the development of improved treatment products". School of physical and chemical sciences, Brisbane, Queensland University of Technology: 195.

Scheuplein, R. J. and I. H. Blank (1971). "Permeability of the skin." Physiol Rev 51(4): 702-747.

Schmook, F. P., J. G. Meingassner, et al. (2001). "Comparison of human skin or epidermis models with human and animal skin in in-vitro percutaneous absorption." International Journal of Pharmaceutics 215(1-2): 51-56.

Schubnell, M., I. Kamber, et al. (1997). "Photochemistry at high temperatures - Potential of ZnO as a high temperature photocatalyst". Applied Physics a-Materials Science & Processing 64(1): 109-113.

Schulz, J., H. Hohenberg, et al. (2002). "Distribution of sunscreens on skin." Advanced Drug Delivery Reviews 54: S157-S163.

Serpone, N., D. Lawless, et al. (1995). "Subnanosecond relaxation dynamics in TiO_2 colloidal sols (particle sizes R(P)=1.0-13.4 nm- relevance to heterogeneous photocatalysis". Journal of Physical Chemistry 99(45): 16655-16661.

Sheppard, C. J. R. and C. J. Cogswell (1991). "Signal strength and noise in confocal microscopy-factors influencing selection of an optimum detector aperture." Scanning 13(3): 233-240.

Sheppard, C. J. R. and M. Gu (1992). "The significance of 3D transfer-functions in confocal scanning microscopy." Journal of microscopy-Oxford 165: 377-390.

Shim, J., H. S. Kang, et al. (2004). "Transdermal delivery of mixnoxidil with block copolymer nanoparticles." Journal of Controlled Release 97(3): 477-484.

Silva, A. F. d., I. Pepe, et al. (2004). "Electronic and optical properties of rutile titanium dioxide". Physica Status Solidi 1(S2): S241-S244.

Sinico, C., M. Manconi, et al. (2005). "Liposomes as carriers for denual delivery of tretinoin: *in vitro* evaluation of drug penneation and vesicle-skin interaction." Journal of Controlled Release 103(1): 123-136.

Smith, A. M., H. W. Duan, et al. (2006). "A systematic examination of surface coatings on the optical and chemical properties of semiconductor quantum dots." Physical Chemistry Chemical Physics 8(33): 3895-3903.

Sniekers, Y. H. and C. C. van Donkelaar (2005). "Determining diffusion coefficients in inhomogeneous tissues using fluorescence recovery after photobleaching." Biophysical Journal 89(2): 1302-1307.

Squirrell, J. M., J. G. White, et al. (1999). "Long-term two-photon fluorescence imaging of mammalian embryos without compromising viability." Nature biotechnology 17(8): 763-762.

Stracke, F., B. Weiss, et al. (2006). "Multiphoton microscopy for the investigation of dermal penetration of nanoparticle-borne drugs." Journal of Investigative Dermatology 126(10): 2224-2233.

Sutherland, R. L. (1996). Handbook of Nonlinear Optics. New York, Marcel Dekker.

Sznitowska, M., S. Janicki, et al. (2001). "Studies on the effect of pH on the lipoidal route of penetration across stratum corneum." J Control Release 76(3): 327-335.

Thong, H. Y., H. Zhai, et al. (2007). "Percutaneous penetration enhancers: an overview." Skin Pharmacol Physiol 20(6): 272-282.

Thune, P., T. Nilsen, et al. (1988). "The water barrier function of the skin in relation to the water content of stratum corneum, pH and skin lipids. The effect of alkaline soap and syndet on dry skin in elderly, non-atopic patients." Acta Derm Venereol 68(4): 277-283.

Tinkle, S. S., J. M. Antonini, et al. (2003). "Skin as a route of exposure and sensitization in chronic beryllium disease." Environmental Health Perspectives 111(9): 1202-1208.

Toll, R., U. Jacobi, et al. (2004). "Penetration profile of microspheres in follicular targeting of terminal hair follicles." Journal of Investigative Dermatology 123(1): 168-176.

Trommer, H. and R. H. H. Neubert (2006). "Overcoming the stratum corneum: The modulation of skin penetration - A review." Skin Pharmacology and Physiology 19(2): 106-121.

Tuchin, V. (2000). Tissue Optics: Light Scattering Methods and Instruments for Medical Diagnosis. Boston, Kluwer Academic Publishers.

van Ravenzwaay, B. and E. Leibold (2004). "The significance of *in vitro* rat skin absorption studies to human risk assessment". Toxicol *In Vitro* 18(2): 219-225.

Vogt, A., B. Combadiere, et al. (2006). "40 nm, but not 750 or 1,500 nm, nanoparticles enter epidermal CD1a+ cells after transcutaneous application on human skin." Journal of Investigative Dermatology 126(6): 1316-1322.

Vos, K. and H. J. Krusemeyer (1977). "Reflectance and electroreflectance of TiO_2 single crystals : I. Optical spectra". Journal of Physics C: Solid State Physics 10: 3893-3915.

Wang, T. F., G. B. Kasting, et al. (2006). "A multiphase microscopic diffusion model for stratum corneum permeability. I. Formulation, solution, and illustrative results for representative compounds." J Pharm Sci 95(3): 620-648.

William J. Mulholland, M. A. K., Brian J. Bellhouse, and Nick White (June 2002). Analysis of microparticle penetration into human and porcine skin: non-invasive imaging with multiphoton excitation microscopy. Multiphoton Microscopy in the Biomedical Sciences II.

Wilson, T. and S. J. Hewlett (1991). "Optical sectioning strength of the direct-view microscope employing finite-sized pinhole arrays." Journal of microscopy-oxford 163: 131-150.

Xu, Z. P., Q. H. Zeng, et al. (2006). "Inorganic nanoparticles as carriers for efficient cellular delivery". Chemical Engineering Science 61(3): 1027-1040.

Yoneto, K., S. K. Li, et al. (1996). "Fluorescent probe studies of the interactions of 1-alkyl-2-pyrrolidones with stratum corneum lipid liposomes." Journal of Pharmaceutical Sciences 85(5): 511-517.

Yu, B., K. H. Kim, et al. (2003). "Visualization of oleic Carboxylic-induced transdermal diffusion pathways using two-photon fluorescence microscopy." Journal of Investigative Dermatology 120(3): 448-455.

Zhang, X. H., S. J. Chua, et al. (2006). "Exciton radiative lifetime in ZnO quantum dots embedded in SiOx matrix." Applied physics letters 88: 221903.

Zheng Yuangang, G. H., Steven Colson (2004). "Multichannel multiphoton imaging of metal oxides particles in biological system " Proceeding of SPIE: 5323-5355.

Zvyagin, A. V., X. Zhao, et al. (2008). "Imaging of Zinc Oxide Nanoparticle Penetration in Human Skin *in vitro* and *in vivo*". Journal of Biomedical Optics in review.